

Energy mechanism of the first-order superradiant phase transition in cavity-BEC system with double asymmetric pump beams

Wei Qin(覃威), Dong-Chen Zheng(郑东琛), Jia-Ying Lin(林佳颖), Yuan-Hong Chen(陈元鸿), and Renyuan Liao(廖任远)

Citation: Chin. Phys. B, 2025, 34 (**12**): 120507. DOI: 10.1088/1674-1056/addeb7
http://cpb.iphy.ac.cn; http://iopscience.iop.org/cpb

What follows is a list of articles you may be interested in

Kármán vortex street in a spin-orbit-coupled Bose-Einstein condensate with PT symmetry

Kai-Hua Shao(邵凯花), Bao-Long Xi(席保龙), Zhong-Hong Xi(席忠红), Pu Tu(涂朴), Qing-Qing Wang(王青青), Jin-Ping Ma(马金萍), Xi Zhao(赵茜), and Yu-Ren Shi(石玉仁)

Chin. Phys. B, 2024, 33 (**6**): 060501. DOI: 10.1088/1674-1056/ad2bf3

Dynamics of bubble-shaped Bose-Einstein condensates on two-dimensional cross-section in micro-gravity environment

Tie-Fu Zhang(张铁夫), Cheng-Xi Li(李成蹊), and Wu-Ming Liu(刘伍明)

Chin. Phys. B, 2023, 32 (**9**): 090501. DOI: 10.1088/1674-1056/acd922

Merging and splitting dynamics between two bright solitons in dipolar Bose-Einstein condensates

Xin Li(李欣), Peng Gao(高鹏), Zhan-Ying Yang(杨战营), and Wen-Li Yang(杨文力)

Chin. Phys. B, 2021, 30 (**12**): 120501. DOI: 10.1088/1674-1056/abff3f

Domain walls and their interactions in a two-component Bose-Einstein condensate

Ling-Zheng Meng(孟令正), Yan-Hong Qin(秦艳红), Li-Chen Zhao(赵立臣), Zhan-Ying Yang(杨战营)

Chin. Phys. B, 2019, 28 (**6**): 060502. DOI: 10.1088/1674-1056/28/6/060502

Solitons in nonlinear systems and eigen-states in quantum wells

Li-Chen Zhao(赵立臣), Zhan-Ying Yang(杨战营), Wen-Li Yang(杨文力)

Chin. Phys. B, 2019, 28 (**1**): 010501. DOI: 10.1088/1674-1056/28/1/010501

Energy mechanism of the first-order superradiant phase transition in cavity-BEC system with double asymmetric pump beams

Wei Qin(覃威)[1,2,†], Dong-Chen Zheng(郑东琛)[1,2,†], Jia-Ying Lin(林佳颖)[1,2], Yuan-Hong Chen(陈元鸿)[1,2], and Renyuan Liao(廖任远)[1,2,‡]

[1] *College of Physics and Energy, Fujian Normal University, Fujian Provincial Key Laboratory of Quantum Manipulation and New Energy Materials, Fuzhou* 350117, *China*

[2] *Fujian Provincial Engineering Technology Research Center of Solar Energy Conversion and Energy Storage, Fuzhou* 350117, *China*

(Received 21 March 2025; revised manuscript received 22 May 2025; accepted manuscript online 30 May 2025)

We consider a Bose–Einstein condensate loaded inside an optical cavity and exposed to two crossed coherent pump fields with same imbalance parameter γ. We identify different effects between pure standing wave fields ($\gamma = 1$) and the pump beams combining standing wave and running wave ($\gamma \neq 1$). In particular, for $\gamma = 1$, the system only hosts a normal phase and a superradiant phase. In contrast, for $\gamma \neq 1$, the system features three distinctive phases: the normal phase (NP), superradiant phase 1 (SR_1), and superradiant phase 2 (SR_2). Importantly, the superradiance is subdivided into different types characterized by the photon phase. Furthermore, we determine perturbatively the phase boundary separating the normal phase and the superradiant phases, and find that there exists a competitive relationship of energy minimum on the overlapping region between SR_1 and SR_2. Interestingly, the transition between the normal phase to SR_1 or SR_2 is identified to be a second-order phase transition, while the transition between SR_1 and SR_2 is a first-order transition. When the first-order phase transition occurs, the phase of the photons changes abruptly from 0 to $\pi/2$.

Keywords: Bose–Einstein condensate, superradiant phase transition, light–atom hybrid system

PACS: 42.50.Pq, 64.70.Tg, 03.75.Nt

DOI: 10.1088/1674-1056/addeb7 **CSTR:** 32038.14.CPB.addeb7

1. Introduction

Loading quantum gases into a high-finesse optical cavity provides fascinating avenues for simulating novel quantum phenomena and exploring many-body physics.[1–14] In such light–atom hybrid systems, the ultracold dilute bosonic or fermionic gases inside an initially unoccupied cavity mode are illuminated by an external pump laser field. When the strength of the pump field exceeds a critical value, the long-range interaction between particles is generated, stemming from the scattering of photons between the transverse pump and the cavity mode via off-resonant Raman processes, and is essential for the realization of fascinating many-body phenomena.[7,15–20] Typically the incident pump consists of a pair of counterpropagating pumping lasers with equal strength, in which case different phases of the system can be distinguished by the arrangement of the atoms since the phase of intracavity photons is constrained to be in either 0 or π.[4,15,21,22] However, employing the unbalanced counterpropagating beams has discernible effects on the phase of intracavity photons, which can be used as a means to discriminate different superradiant phases of the system.[23,24]

The system undergoes a superradiant phase transition from the normal phase into the self-ordered state on the condition that the gain in potential energy is able to overcome the loss in kinetic energy.[15] At the transition point the collective excitation mode softens at the coupled momentum, and regularly distributed atoms in emerging intracavity light field can further reduce their energy.[16,25–27] For red detuning, the atoms are in *S* orbitals due to the scattering terms being even spatial symmetry. In contrast, in the blue-detuned regime, the atoms are able to be scattered to higher orbital bands due to the odd spatial symmetry of the scattering terms.[28,29] In addition, the spatial arrangement of atoms leads to destructive interferences, which lowers the repulsive pump lattice potential and allows quantum phase transitions to occur in the repulsive potential.[23,24,28–31]

Such studies utilizing unbalanced counterpropagating beams in the case of blue detuning are common. Accompanying the deep research of cavity-QED in the field of quantum simulation, it has become appealing to introduce multiple cavities or pump beams in the settings.[9,32–37] Our model integrates the configurations from Ref. [23] (a single unbalanced pump beam) and Ref. [33] (two single-mode cavities), investigating phase transitions when replacing two cavities with two pump beams under unbalanced conditions (see Fig. 1(a)). By constructing phase diagrams, we conclude that the system does not experience suppression of intracavity photons in the region of equal intensities compared to the two pairs of bal-

[†] These authors contributed equally to this work.

[‡] Corresponding author. E-mail: ryliao@fjnu.edu.cn

© 2025 Chinese Physical Society and IOP Publishing Ltd. All rights, including for text and data mining, AI training, and similar technologies, are reserved.

anced beams, and an energy minimum occurs in this region only when the photon phase is $\pi/2$. We find that there is a first-order transition employing an asymmetric pump beam, and that the first-order phase transition occurs at the swap between a local energy minimum and the global energy minimum.

2. Model

We consider that a spinless Bose–Einstein condensate (BEC) is trapped inside a high-finesse optical cavity, and are illuminated by two pairs of pump beams that are a mixture of standing and running waves. As shown in Fig. 1(a), the angle between the cavity axis and per pump beam is 60°. The wave vectors of the cavity light and the pump beams are given by $\boldsymbol{k}_{\rm c} = k_0\hat{\boldsymbol{e}}_x$ and $\boldsymbol{k}_j = (-1)^j k_0 \sin(60^\circ)\hat{\boldsymbol{e}}_x + k_0\cos(60^\circ)\hat{\boldsymbol{e}}_y$ with $j = \{1,2\}$. Here j is the identifier of the different pumps and k_0 is the wave-vector magnitude of the pumping lasers and the cavity mode. The interaction between atoms and light can be understood from the scalar atomic polarizability, $\hat{H}_{\rm A-L} = -\hbar\hat{\boldsymbol{E}}^\dagger\cdot\hat{\boldsymbol{E}}/\Delta_{\rm a}$,[38–41] so that the many-body Hamiltonian in a frame rotating with the pump laser frequency reads

$$\hat{\mathcal{H}} = -\hbar\Delta_{\rm c}\hat{a}^\dagger\hat{a} + \int {\rm d}\boldsymbol{r}\hat{\Psi}^\dagger(\boldsymbol{r})\left(\frac{\hat{\boldsymbol{p}}^2}{2M} + \hat{H}_{\rm A-L}\right)\hat{\Psi}(\boldsymbol{r}), \quad (1)$$

where $\Delta_{\rm a} = \omega_{\rm p} - \omega_{\rm a}$ and $\Delta_{\rm c} = \omega_{\rm p} - \omega_{\rm c}$ are the atom–pump detuning and the cavity–pump detuning, respectively. We consider the pump beams that have the same frequency $\omega_{\rm p}$ and they are detuned far from the atomic resonance frequency $\omega_{\rm a}$ to ensure that the electronic excitation is sufficiently small and the upper atomic excited state can be eliminated adiabatically. We assume that the cavity frequency is closely detuned from the pump frequency. $\hat{\Psi}^\dagger$ ($\hat{\Psi}$), $\hat{a}^\dagger$ ($\hat{a}$), $\hat{\boldsymbol{p}} = -{\rm i}\hbar\nabla$ denotes atomic creation (annihilation) operator with mass M, photon creation (annihilation) operator and atomic momentum operator, respectively. Here $\hat{\boldsymbol{E}} = \hat{\boldsymbol{E}}_{\rm c} + \sum_j \boldsymbol{E}_{{\rm p}j}$ is the total electric field operator and the quantized electric field of the cavity is given by $\hat{\boldsymbol{E}}_{\rm c} = E_0\cos(\boldsymbol{k}_{\rm c}\cdot\boldsymbol{r})\hat{a}\hat{\boldsymbol{e}}_z$, where E_0 is the electric field strength of a single cavity photon. It is worth emphasizing that the pump field originating from two unbalanced counterpropagating beams can be described as $\boldsymbol{E}_{{\rm p}j} = \hat{\boldsymbol{e}}_z(E_{j+}{\rm e}^{{\rm i}\boldsymbol{k}_{{\rm p}j}\cdot\boldsymbol{r}} + E_{j-}{\rm e}^{-{\rm i}\boldsymbol{k}_{{\rm p}j}\cdot\boldsymbol{r}})/2$, where $E_{j\pm}$ represents the strong (+) or weak (−1) amplitude of pump field j. Substituting the total electric field operator $\hat{\boldsymbol{E}}$ into the Eq. (1), we find that the Hamiltonian of the atom–light interaction consists of the following six terms:

$$\hat{H}_{\rm A-L} = \hat{H}^{\rm c}_{\rm pot} + \hat{H}^{\rm interf}_{\rm p1-p2} + \sum_{j=1,2}\{\hat{H}^{\rm pj}_{\rm pot} + \hat{H}^{\rm coupl}_{{\rm p}j-c}\}, \quad (2)$$

where

$$\begin{aligned}
\hat{H}^{\rm c}_{\rm pot} &= U_0\hat{a}^\dagger\hat{a}\cos^2(\boldsymbol{k}_{\rm c}\cdot\boldsymbol{r}),\\
\hat{H}^{\rm pj}_{\rm pot} &= V_j\cos^2(\boldsymbol{k}_j\cdot\boldsymbol{r}),\\
\hat{H}^{\rm interf}_{\rm p1-p2} &= \frac{\sqrt{V_1V_2}}{2}\left\{\left(\gamma+\frac{1}{\gamma}\right)\cos\left[(\boldsymbol{k}_1-\boldsymbol{k}_2)\cdot\boldsymbol{r}\right]\right.\\
&\quad \left.+2\cos\left[(\boldsymbol{k}_1+\boldsymbol{k}_2)\cdot\boldsymbol{r}\right]\right\},\\
\hat{H}^{\rm coupl}_{{\rm p}j-c} &= \eta_{j+}(\hat{a}^\dagger+\hat{a})\cos(\boldsymbol{k}_j\cdot\boldsymbol{r})\cos(\boldsymbol{k}_{\rm c}\cdot\boldsymbol{r})\\
&\quad +\eta_{j-}(\hat{a}^\dagger-\hat{a}){\rm i}\sin(\boldsymbol{k}_j\cdot\boldsymbol{r})\cos(\boldsymbol{k}_{\rm c}\cdot\boldsymbol{r}). \quad (3)
\end{aligned}$$

In the above expressions, $V_j = E_{j+}E_{j-}/\Delta_{\rm a}$ are optical lattice depth for pump j and $U_0 = E_0^2/\Delta_{\rm a}$ is potential depth for the cavity. The first and second terms in Eq. (3) are the intracavity lattice and transverse pump lattice potentials, while the third term and the last term belongs to the coherence between the pump lights and the two-photon scattering process between the pump lights and the cavity field, respectively. Here $\eta_{j\pm} = \sqrt{U_0V_j}(\gamma\pm1/\gamma)/2$ are the amplitudes of the interference between the pump lights and the cavity field with $\gamma = (E_{j+}/E_{j-})^{1/2}$ being the imbalance parameter. In this study, we require two pairs of unbalanced counterpropagating pumps to have the same γ, choose the recoil energy $E_{\rm r} = \hbar^2k_0^2/2M$ as the basic energy unit and set $\hbar = 1$ from now on for brevity.

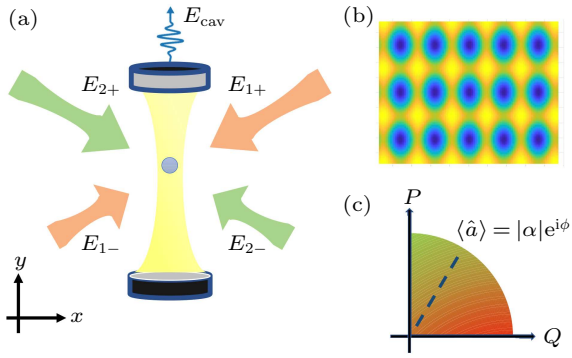


Fig. 1. (a) Schematic diagram of the experimental setup. Ultracold atoms (blue) in a BEC state are placed in a single-mode optical cavity and driven by two pairs of asymmetric pump laser beam 1 (orange) and pump laser beam 2 (green) with the same unbalanced parameter γ. The cavity mode with coherent field amplitude α can be detected in superradiant phases. (b) The atomic density modulation for two unbalanced pump beams without the intracavity field. It exhibits periodic spatial patterns. Here, we can define the reciprocal lattice vector $\boldsymbol{G}_{KL} = K(\boldsymbol{k}_1-\boldsymbol{k}_2) + L(\boldsymbol{k}_1+\boldsymbol{k}_2)$ with K and L are integer. (c) The expectation value of intracavity photons, $\hat{a} = \alpha = |\alpha|{\rm e}^{{\rm i}\phi}$, is described in the complex plane, where ϕ is the phase of the photons. $\hat{Q} = (\hat{a}^\dagger+\hat{a})/2$ and $\hat{P} = {\rm i}(\hat{a}^\dagger-\hat{a})/2$ are orthogonal to each other. The phase angle ϕ is zero when the dashed line falls exactly on the Q axis, while ϕ is $\pi/2$ for the dashed line on the P axis.

In general, the phase transition between the normal phase and the superradiant phase is judged by the presence or absence of intracavity photons. In the normal phase where $\langle\hat{a}\rangle = 0$, the atoms feel an optical lattice consisting of two pairs of unbalanced pump fields and are localized at the position corresponding to the minimum of the lattice potential energy. Figure 1(b) shows the arrangement of these particles in real space, which enjoys the translational symmetry of $2\pi/(\sqrt{3}k_0)$ and $2\pi/k_0$ along the horizontal direction and the vertical direction, respectively. As $\hat{Q} = (\hat{a}^\dagger+\hat{a})/2$ and $\hat{P} = {\rm i}(\hat{a}^\dagger-\hat{a})/2$ are

orthogonal quadratures of the cavity field, by which the expectation value of the cavity field operator can be represented as a complex value [see Fig. 1(c)], $\langle\hat{a}\rangle = \alpha = |\alpha|\mathrm{e}^{\mathrm{i}\phi}$. Except for $|\alpha|$, which serves as an order parameter for distinguishing between the normal phase and the superradiant phase, the phase ϕ is capable of further subdividing the superradiant phase. For $\phi = 0$, the coupling term which is proportional to $\hat{P}$ is always zero, such that the superradiant phase is coupled to the standing wave of pump via the term $\sum_j \cos(\boldsymbol{k}_j \cdot \boldsymbol{r})$. Conversely, when $\phi = \pi/2$, the superradiant phase is coupled to the running wave of pump via the term $\sum_j \sin(\boldsymbol{k}_j \cdot \boldsymbol{r})$. Furthermore, for $0 < \phi < \pi/2$, it is evident that the two couplings can exist simultaneously. We refer to these three types of superradiant phases as superradiant phase 1 (SR_1), superradiant phase 2 (SR_2), and mixed phase (MP) based on the differences in phase ϕ. In particular, SR_1 is coupled with the standing wave of the pumps while SR_2 is coupled with the traveling wave of the pumps. Interestingly, subsequent studies does not reveal the existence of the mixed phase.

3. Theory and method toward a steady solution

The dynamics of such a cavity–atom hybrid system is governed by the Heisenberg equations of motion for atomic and photonic field operators. To seek a steady-state solution with mean-field approximation, we formally replace the operators $\hat{\Psi}$ and $\hat{a}$ with the atomic mean-field $\sqrt{N}\psi_0$ and the coherent complex expectation value α with N being the number of atoms. As the dynamical evolution of the cavity field is very rapid compared to the center of mass motion of the atoms, its dynamical processes can be adiabatically eliminated, i.e., $\mathrm{i}\hbar\partial\hat{a}/\partial t = 0$. Meanwhile, the evolution of the condensate wave function is governed by the Gross–Pitaevskii-type equation, including the mechanical effects of the radiation field inside the cavity.[25,42–44] Thus, the coupled mean-field equations that the system obeys can be written as

$$\alpha = \frac{\Theta_+ + \mathrm{i}\Theta_-}{(\Delta_\mathrm{c} - U_0\mathcal{B}) + \mathrm{i}\kappa}, \tag{4a}$$

$$\mu_0\psi_0 = \left[\frac{\hat{\boldsymbol{p}}^2}{2M} + \hat{H}_{\mathrm{A-L}}(\alpha^*, \alpha)\right]\psi_0. \tag{4b}$$

Here, the cavity decay rate κ originates from the leakage of intracavity photons. The bunching parameter $\mathcal{B} = \int \mathrm{d}\boldsymbol{r}\langle\hat{\Psi}^\dagger(\boldsymbol{r})\hat{B}\hat{\Psi}(\boldsymbol{r})\rangle$ with $\hat{B} = \cos^2(\boldsymbol{k}_\mathrm{c}\cdot\boldsymbol{r})$. We have defined operators $\hat{\Theta}_+$ and $\hat{\Theta}_-$ as $\hat{\Theta}_+ = \sum_{j=1,2}\eta_{j+}\cos(\boldsymbol{k}_j\cdot\boldsymbol{r})\cos(\boldsymbol{k}_\mathrm{c}\cdot\boldsymbol{r})$ and $\hat{\Theta}_{j-} = \sum_{j=1,2}\eta_{j-}\sin(\boldsymbol{k}_j\cdot\boldsymbol{r})\cos(\boldsymbol{k}_\mathrm{c}\cdot\boldsymbol{r})$, respectively, similarly $\Theta_+ = \int \mathrm{d}\boldsymbol{r}\langle\hat{\Psi}^\dagger(\boldsymbol{r})\hat{\Theta}_+\hat{\Psi}(\boldsymbol{r})\rangle$ and $\Theta_- = \int \mathrm{d}\boldsymbol{r}\langle\hat{\Psi}^\dagger(\boldsymbol{r})\hat{\Theta}_-\hat{\Psi}(\boldsymbol{r})\rangle$. μ_0 is the chemical potential and $\hat{H}_{\mathrm{A-L}}(\alpha^*, \alpha)$ is the resultant Hamiltonian obtained by the replacement of $\hat{a}$ ($\hat{a}^\dagger$) with α (α^*) in Eq. (2).

In Landau's phase transition paradigm,[45,46] the ground-state energy of the system is a global minimum. We consider two ways to obtain the system's ground state. The first strategy stems from the split-operator pseudospectral method,[25,47–49] where we propagate ψ_0 in imaginary time according to Eq. (4b), with cavity field replaced by Eq. (4a). The second strategy for searching the lowest ground energy is performing the point-by-point scanning,[23] where the ground-state energy of many-body system is evaluated as $E_\mathrm{g} = N\mu_0 - \Delta_\mathrm{c}|\alpha|^2$ from Eq. (1) and can be plotted as a function of the cavity field quadratures P and Q, then we survey exactly the global minima of ground energy in relation to photon (see Figs. 5(a)–5(e)).

The first strategy is fast but may suffer from errors. When the ground-state energy landscape possesses multiple minima, the problem is that it may search for a solution that is a local minima of the energy, depending on the choice of the initial value. Meanwhile, the second strategy is slow but the result is exact. Based on their strengths, the former is used for line drawings (see Figs. 2 and 5(f)–5(j)) and the latter is used for three-dimensional (3D) drawings (see Figs. 3, 4(c), 4(e) and 5(a)–5(e)).

Inspection of Eq. (4a) indicates that both the order parameters Θ_+ and Θ_- affect the expectation value of cavity field operator, and α can be real of purely imaginary only if the two order parameters are simultaneously nonzero. The property of the complex number can be captured by the phase ϕ of the intracavity photons. In order to clear up the relationship between ϕ and Θ_+, Θ_-, we plot the behavior of the lattice potential in the cavity $U_0|\alpha^2|$ and Θ_+, Θ_- as a function of the pump lattice strength V_1 (see Fig. 2).

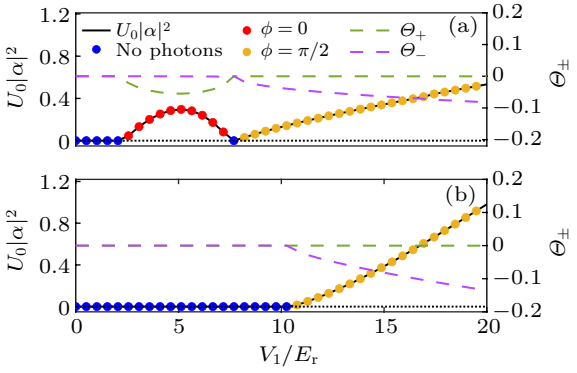


Fig. 2. The order parameters Θ_+ and Θ_- are plotted as a function of the pump lattice depth V_1/E_r, and the corresponding intracavity lattice depth $U_0|\alpha|^2$ are displayed by the black line with (a) $V_2/E_\mathrm{r} = 0$ and (b) $V_2/E_\mathrm{r} = V_1/E_\mathrm{r}$. On the lines, different colored circles imply the phase of the intracavity photon at occupied point: the blue circles is the absence of photons and the red circles is $\phi = 0$ and the orange circles is $\phi = \pi/2$. The green dashed line and purple one are the order parameters Θ_+ and Θ_-, respectively. Parameters used: $N = 4.4\times10^5$, $\Delta_\mathrm{c}/\omega_\mathrm{r} = -8\times10^3$, $U_0/\omega_\mathrm{r} = 0.0126$, $\kappa/\omega_\mathrm{r} = 39$, and $\gamma = 1.28$. These parameters listed above do not change if not explicitly emphasized.

We find that Θ_+ is not zero accompanied by $\phi = 0$, Θ_- is not zero accompanied by $\phi = \pi/2$, and the two parameters cannot exist at the same time. This result is acceptable although it seems to contradict Eq. (4a). Cavity decay can be neglected, since the parameters used in our study, $|\Delta_\mathrm{c} - U_0\mathcal{B}|^2 \gg \kappa^2$, it only leads to a minor shift of α involving

κ. Thus, Θ_+ and Θ_- dominate real and imaginary parts of α, respectively. The two parameters cannot be finite at the same time, which demonstrates the subdivision of the superradiant phase does not include the presence of MP.

We find that Θ_+ and Θ_- are negative, which leads to α is positive due to $(\Delta_c - U_0\mathcal{B}) < 0$ (see Eq. (4a)). This suggests that the phase appearing in $\phi = \pi$ or $\phi = 3\pi/2$ are rationality ignored (see the supplement of Ref. [23]). The parity of the scattering terms reflects the atoms scattering from the S band to higher bands or remaining in the S band.[50] In Eq. (3), the atoms couple to spatial patterns with different parities, which indicates that $\eta_{j+}(\alpha^\dagger + \alpha)$ is more strongly coupled to the second (P) band compared to the first (S) band.[29] In contrast, $\eta_{j-}(\alpha^\dagger - \alpha)$ coupled more strongly to the first (S) band compared to the second (P) band.

We are curious about what different results would be obtained between two pump beams with pure standing wave and two pairs of pump beams with traveling and standing wave components, such two types of pump fields can be analog by setting γ to 1 or not. As shown in Fig. 3, the phase diagrams depicted by the intracavity lattice potentials $U_0|\alpha|^2$ in the plane of the parameters V_1 and V_2, and draw the corresponding phase ϕ of the photons. Here we only consider the case where $\Delta_c < 0$, since the opposite case, $\Delta_c > 0$, leads to the existence of a transition from metastable regime to unstable regime.[28]

Figures 3(a) and 3(c) depict the 3D distribution of the intracavity lattice depth $U_0|\alpha|^2$ across the V_1–V_2 parameter plane for $\gamma = 1$ and $\gamma \neq 1$ cases respectively, with Figs. 3(b) and 3(d) displaying their two-dimensional (2D) cross-sections. The colored regions in Figs. 3(b) and 3(d) indicate the presence of photons, where hue variations encode the photon phase differences. We find that as V_2 gradually approaches $2E_r$ from 0, the threshold pump strength V_1 required for the emergence of intracavity lattice depth increases, indicating an increased difficulty for the system to enter the superradiant phase. For $V_2 \in [2E_r, 7E_r]$, the systems first transition from the superradiant phase to the normal phase and then re-enter the superradiant phase as V_1 increases. The significant differences between the two cases are: for $\gamma = 1$, the intracavity photon is suppressed near $V_1 = V_2$, and the system exhibits only a $\phi = 0$ superradiant phase; for $\gamma \neq 1$, intracavity photon population is allowed near the $V_1 = V_2$ condition, and the superradiant phase admits additional phases (e.g., $\phi = \pi/2$).

Figures 3(a)–3(d) are symmetric along $V_1 = V_2$, which means it is equivalent to fix one of pump depths while varying the other. Meanwhile, it illustrates that the pump field of standing wave produces self-ordering phase with only real expectation value of intracavity photon, and the pump field of traveling wave produces a self-ordering phase with purely imaginary expectation value of intracavity photon. For the case of blue detuning $\Delta_a > 0$, the self-ordering phase around $V_1 = V_2$ is coupled to the traveling wave. The dashed arrows in Fig. 3(d) point out the most interesting difference between $\gamma = 1$ and $\gamma \neq 1$.

Figure 3(e) illustrates the effects of Δ_c and γ on the phase boundary along $V_1 = V_2$ at $\gamma \neq 1$. For the larger of γ, the smaller the optical lattice depth of pumps are required for the transition of NP into SR_2 at a certain cavity–pump detuning Δ_c on the one hand. On the other hand, for the larger of Δ_c, the contrary the optical lattice depth of pumps are required for this transition at a certain imbalance parameter γ.

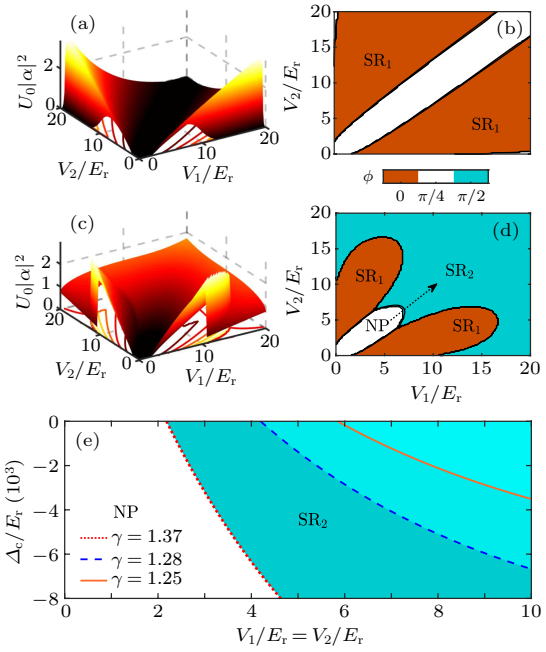


Fig. 3. From the amplitude $|\alpha|$ we calculated the intracavity lattice depth $U_0|\alpha|^2$ for (a) $\gamma = 1$ and (c) $\gamma = 1.28$ with the same cavity detuning $\Delta_c = -5 \times 10^3 E_r$; their corresponding phase of the light field mapped to the first quadrant ($\phi = [0, \pi/2]$) is shown in panels (b) and (d) respectively. (e) Phase diagram spanned by pump lattice depths with same strength ($V_1/E_r = V_2/E_r$) and the cavity detuning $\Delta_c/E_r(\times 10^3)$. Dotted, dashed, and solid lines are numerical results of the imbalance parameter $\gamma = 1.37$, 1.28, and 1.25, respectively. The acronyms NP, SR_1, and SR_2 stand for the normal phase, superradiance 1, and superradiance 2, respectively.

4. Energy mechanism of the first-order superradiant phase transition

The order parameters Θ_+ and Θ_- can be well used to subdivide the superradiant phase, here, $\Theta_+ \neq 0$ but $\Theta_- = 0$, $\Theta_+ = 0$ but $\Theta_- \neq 0$, and both $\Theta_+ \neq 0$ and $\Theta_- \neq 0$, which correspond to SR_1, SR_2, and MP, respectively. At the vicinity of the critical point, we can treat the terms in Eq. (1) involving $\hat{a}$ ($\hat{a}^\dagger$) as a perturbation since the photon number is very small.

At the zero-temperature limit, all atoms occupy the lowest-energy state, so that the atomic field operator can be expanded with a set of Bloch wave solutions of the unperturbed Hamiltonian $\hat{H}_0$

$$\hat{\Psi}(\boldsymbol{r}) = \left\langle \boldsymbol{r}|\Psi^{(1)}(0)\right\rangle \hat{b}_{0,1} + \sum_{m,\boldsymbol{k}\neq 0} \left\langle \boldsymbol{r}|\Psi^{(m)}(\boldsymbol{k}))\right\rangle \hat{b}_{\boldsymbol{k},m}, \quad (5)$$

where

$$\hat{H}_0 = \int \mathrm{d}\boldsymbol{r}\hat{\Psi}^\dagger(\boldsymbol{r})\left(\frac{\hat{\boldsymbol{p}}^2}{2M} + \sum_{j=1,2}\hat{H}^{\mathrm{pj}}_{\mathrm{pot}} + \hat{H}^{\mathrm{interf}}_{\mathrm{p1-p2}}\right)\hat{\Psi}(\boldsymbol{r}). \quad (6)$$

Here $|\Psi^{(m)}(\boldsymbol{k})\rangle$ denotes the Bolch state with quasi-momenta $\boldsymbol{k}$ and band index m, and $|\Psi^{(1)}(0)\rangle$ is the lowest-energy Bloch state. $\hat{b}_{0,1}$ is the annihilation operator for state $|\Psi^{(1)}(0)\rangle$ and $\hat{b}_{\boldsymbol{k},m}$ is the annihilation operator for state $|\Psi^{(m)}(\boldsymbol{k})\rangle$ ($\boldsymbol{k} \neq 0$). Noteworthy, all possible two-photon processes coherently couple the zero-momentum state of the BEC $|k_x,k_y\rangle = |0,0\rangle$ to the twelve momentum-states, $|k_x,k_y\rangle = |\pm\boldsymbol{k}_c \pm \boldsymbol{k}_j\rangle$ and $|k_x,k_y\rangle = |\pm\boldsymbol{k}_1 \pm \boldsymbol{k}_2\rangle$. We take into account the symmetry of the energy band structure to simplify the calculation, hence it is reasonable to use the momentum $\boldsymbol{k}_1 = \boldsymbol{k}_c - \boldsymbol{k}_2$ to replace all possible momentums in the second term of Eq. (5).

Substituting the atomic field operator into Eq. (1) results in the effective Hamiltonian

$$\begin{aligned}\hat{H}_{\mathrm{eff}} =& -\tilde{\Delta}_c\hat{a}^\dagger\hat{a} + \sum_m (E_{\boldsymbol{k}_1,m} - E_{0,1})\hat{b}^\dagger_{\boldsymbol{k}_1,m}\hat{b}_{\boldsymbol{k}_1,m} \\ &+ (\hat{a}^\dagger + \hat{a})\sum_m(\theta_{m,+}\hat{b}^\dagger_{0,1}\hat{b}_{\boldsymbol{k}_1,m} + \mathrm{H.c.}) \\ &+ \mathrm{i}(\hat{a}^\dagger - \hat{a})\sum_m(\theta_{m,-}\hat{b}^\dagger_{0,1}\hat{b}_{\boldsymbol{k}_1,m} + \mathrm{H.c.}), \end{aligned} \quad (7)$$

where $\tilde{\Delta}_c = \Delta_c - U_0\langle\Psi^{(1)}(0)|\hat{B}|\Psi^{(1)}(0)\rangle$ is dispersive shift cavity detuning. $E_{0,1}$ and $E_{\boldsymbol{k}_1,m}$ are eigenvalues of $\hat{H}_0$ corresponding to eigenvectors $|\Psi^{(1)}(0)\rangle$ and $|\Psi^{(m)}(\boldsymbol{k}_1)\rangle$, respectively. The scattering matrix elements are given by $\theta_{m,+} = \langle\Psi^{(1)}(0)|\hat{\Theta}_+|\Psi^{(m)}(\boldsymbol{k}_1)\rangle$, and the other as $\theta_{m,-} = \langle\Psi^{(1)}(0)|\hat{\Theta}_-|\Psi^{(m)}(\boldsymbol{k}_1)\rangle$. In the derivation, the particle number conservation $\hat{b}^\dagger_{0,1}\hat{b}_{0,1} + \sum_m \hat{b}^\dagger_{\boldsymbol{k}_1,m}\hat{b}_{\boldsymbol{k}_1,m} = N$ should be satisfied, and the summation are carried over all band indices.

We implement the mean-field theory by replacing the atomic operators and photon operator by their average values $\hat{b}_{0,1} = \psi_{0,1}$, $\hat{b}_{\boldsymbol{k}_1,m} = \psi_{\boldsymbol{k}_1,m}$, and $\hat{a} = \alpha$. We seek a steady state in which $\partial_t\psi_{\boldsymbol{k}_1,m} = 0$ with $\mathrm{i}\partial_t\hat{b}_{\boldsymbol{k}_1,m} = [\hat{b}_{\boldsymbol{k}_1,m}, \hat{H}_{\mathrm{eff}}]$ and obtain $\psi_{\boldsymbol{k}_1,m} = -\left[(\alpha^*+\alpha)\theta^*_{m,+} + \mathrm{i}(\alpha^*-\alpha)\theta^*_{m,-}\right]\psi_{0,1}/(E_{\boldsymbol{k}_1,m} - E_{0,1})$. Together with the normalization condition $|\psi_{0,1}|^2 = N - \sum_m|\psi_{\boldsymbol{k}_1,m}|^2$. Substituting these expressions into Eq. (7) and obtaining the ground-state energy up to the fourth order in the photon field amplitudes α

$$\begin{aligned}\mathcal{E}(\alpha^*,\alpha) =& -\tilde{\Delta}_c\alpha^*\alpha - N[(\alpha^*+\alpha)^2\chi_1 - (\alpha^*-\alpha)^2\chi_2] \\ &+ N(\alpha^*+\alpha)^4\chi_1\nu_1 + N(\alpha^*-\alpha)^4\chi_2\nu_2 \\ &- N(\alpha^*+\alpha)^2(\alpha^*-\alpha)^2(\chi_1\nu_2 + \chi_2\nu_1), \end{aligned} \quad (8)$$

two susceptibilities are $\chi_1 = \sum_m|\theta_{m,+}|^2/(E_{\boldsymbol{k}_1,m} - E_{0,1})$ and $\chi_2 = \sum_m|\theta_{m,-}|^2/(E_{\boldsymbol{k}_1,m} - E_{0,1})$. We have introduce two symbols $\nu_1 = \sum_m|\theta_{m,j+}|^2/(E_{\boldsymbol{k}_1,m} - E_{0,1})^2$ and $\nu_2 = \sum_m|\theta_{m,j-}|^2/(E_{\boldsymbol{k}_1,m} - E_{0,1})^2$ for compact notations. The scattering matrix elements obey $\theta_{m,+}\theta^*_{m,-} + \theta^*_{m,+}\theta_{m,-} = 0$. In the above discussion, equation (4a) informs us about the valuer of α in the steady condition, and we obtain $\alpha = (\Theta_+ + \mathrm{i}\Theta_-)/\tilde{\Delta}_c$ by reasonably neglecting κ. So the ground-state energy becomes

$$\begin{aligned}\mathcal{E}(\Theta_+,\Theta_-) =& -\frac{1}{\tilde{\Delta}_c}(\tilde{\Delta}_c + 4N\chi_1)\Theta_+^2 - \frac{1}{\tilde{\Delta}_c}(\tilde{\Delta}_c + 4N\chi_2)\Theta_-^2 \\ &+ \frac{16N\chi_1\nu_2 + \chi_2\nu_1}{\tilde{\Delta}_c^4}\Theta_+^2\Theta_-^2 \\ &+ \frac{16N\chi_1\nu_1}{\tilde{\Delta}_c^4}\Theta_+^4 + \frac{16N\chi_2\nu_2}{\tilde{\Delta}_c^4}\Theta_-^4. \end{aligned} \quad (9)$$

Some comments are in order. Firstly, as equation (7) is invariant under the simultaneous transformation $\hat{a} \to -\hat{a}$ and $\hat{b}_{\boldsymbol{k}_1,m} \to -\hat{b}_{\boldsymbol{k}_1,m}$, the system spontaneously breaks $\mathcal{Z}_2$ symmetry during the transition from the normal phase to superradiance phase.[51] Secondly, in Eq. (9), the coefficients of the fourth-order terms being positive ensures the stability of the system, while the coefficients of the second-order terms being positive or negative cause the minimization of the ground state energy to occur at α being zero or finite with the former case corresponding to the normal phase and the latter case to the superradiant phase. Accordingly, yielding the established superradiant phase condition

$$-\frac{4N\chi_1}{\tilde{\Delta}_c} > 1, \quad (10a)$$

$$-\frac{4N\chi_2}{\tilde{\Delta}_c} > 1, \quad (10b)$$

here, equation (10a) corresponding to Θ_+ is finite and equation (10b) corresponding to Θ_- is finite.

The key part of the phase transition condition is the two susceptibilities, which characterizes the tendency of inducing superradiance $\phi = 0$ or $\phi = \pi/2$. In Figs. 4(a) and 4(b), we present the numerical results for χ_1 and χ_2 at zero temperature with $\gamma = 1.37$. The difference between the two graphs lies in two aspects. One is the position of the maximum value in the plane: as V_1 and V_2 gradually increase, the maximum of χ_1 moves closer to the center axis, but the maximum of χ_2 is always close to both axes. The other is the value around $V_1 = V_2$: χ_1 tends to zero, while χ_2 is larger. Their similarity is not obvious but traceable. When the value of V_2 is large, χ_1 and χ_2 follow the tendency of increasing firstly and then decreasing, and the descending rate is rapid in Fig. 4(a) but the ascending rate is quick in Fig. 4(b).

Solving the phase transition condition Eqs. (10a) and (10b) with respect to Δ_c yields the critical cavity detuning

$$\Delta_{c,l} = U_0\langle\Psi^{(1)}(0)|\hat{B}|\Psi^{(1)}(0)\rangle - 4N\chi_l, \quad (11)$$

where $\Delta_{c,l}$ is the pump–cavity detuning for the difference susceptibilities χ_l, with $l = 1,2$.

A larger χ_l indicate a greater critical magnitude of the cavity detuning $\Delta_{c,l}$. We map out the phase diagrams spanned by V_1 and Δ_c at $V_2 = 0$. On one hand it is consistent with the results of Ref. [23], proving the correctness of methods. On the

other hand, we find the connection between the analytical and numerical solutions through the phase diagrams. The boundary between the normal phase and superradiance is perfectly matched [see Figs. 4(c) and 4(d)]. However, the subdivision for the superradiant phase is not satisfactory due to the fact that the curve of critical cavity detuning corresponding to χ_1 and the curve of critical cavity detuning corresponding to χ_2 have both overlapping and independent regions [see Fig. 4(d): the non-overlapping dark-red is region SR_1, light-blue is region SR_2, and the gray indicates the overlapping region].

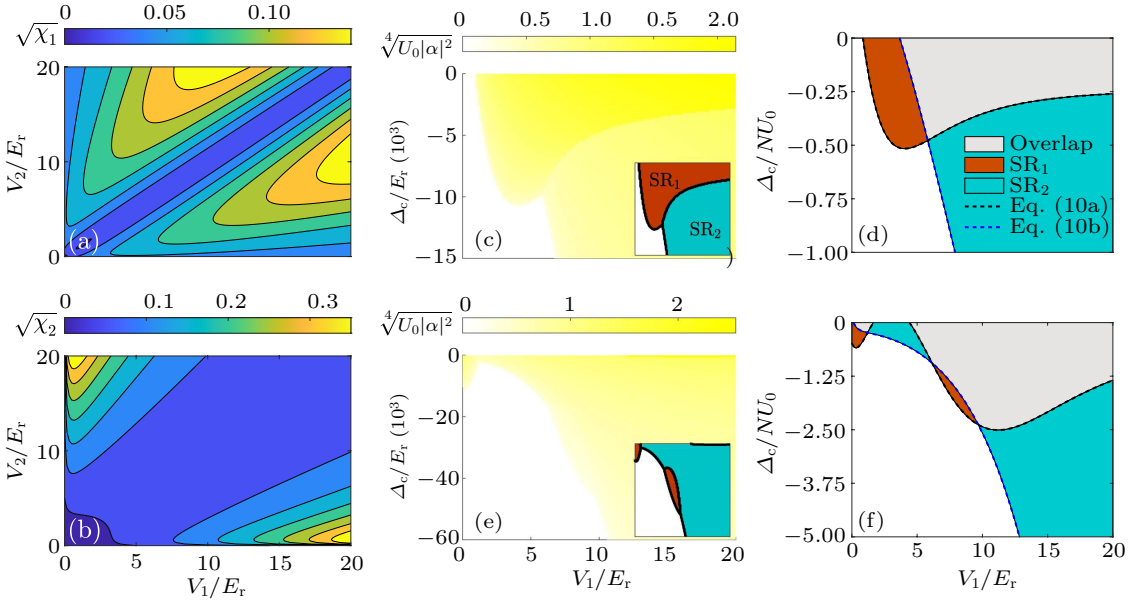


Fig. 4. Square root of the dimensionless susceptibilities χ_1 and χ_2 as a function of V_1/E_r and V_2/E_r is shown in panels (a) and (b), respectively. The brightness of the region is proportional to the magnitude of χ_1 (χ_2): a brighter region represents a larger χ_1 (χ_2). Panels (c) and (e) show $\sqrt[4]{U_0|\alpha|^2}$ as a function of one of the pump lattice depth V_1/E_r and cavity detuning $\Delta_c/E_r(\times 10^3)$. These two images have the same imbalance parameter $\gamma = 1.37$ and are depicted at $V_2/E_r = 0$, 3. The insert shows the calculated phase of the light field in the same parameter range. Dashed–dotted lines are hypothetical boundaries of SR_1 (balck dashed–dotted line) and SR_2 (dark–blue dashed–dotted line) from Eqs. (10a) and (10b) for (d) $V_2/E_r = 0$ and (f) $V_2/E_r = 3$. Panels (d) and (f) correspond to the numerical results of panels (c) and (e), respectively. The white regions are normal phase, the dark–red regions are superradiance SR_1 without overlapping part and light–blue regions are SR_2 without overlapping part. The gray regions are the overlapping part and suggest that there exists competition of minimum energy between SR_1 and SR_2. The acronyms are set to be the same as shown in Fig. 3, and the color marking is the same between panels (d) and (f).

Subdividing the independent regions is effortless, as they can be understood by what phases of intracavity photons can be allowed to occur inside the areas. At first glance, the gray regions imply that photons of the two phases $\phi = 0$ and $\phi = \pi/2$ are capable of coexisting, and the superradiance of the system is mixed phase in this region, where the atoms feel the coupling from both standing and traveling waves. This is not the case, however, the inset in Fig. 4(c) demonstrates that the gray region is completely occupied by SR_1. In order to clarify the attribution of the overlapping region, we plot the phase diagrams at $V_2 = 3$ for comparisons [see Figs. 4(e) and 4(f)]. Identically, the boundary between the normal phase and superradiant phase has the same tendency for both numerical and analytical solutions. However, the overlapping region is almost entirely occupied by the superradiant phase SR_2. This implies that the gray region has a competitive relationship of ground-state energy minimum for intracavity photons of the phases $\phi = 0$ and $\phi = \pi/2$. In contrast, for the normal phase and independent regions [see Figs. 4(d) and 4(f)], white directly indicates that the minimum energy occurs at the photon number being zero, and the dark–red and light–blue indicate that the expectation value α is real and pure imaginary, respectively.

The underlying algorithm for numerical simulation is to search for the global minimum of the ground-state energy of the system. To make clear of what is this energy trend on both sides of and at the point of phase boundaries. In other words, we want to sort out whether the transition between normal phase and superradiance is the first order or the second order, and similarly we want to sort out whether the transition between SR_1 and SR_2 is the first order or the second order. The zero-temperature energy landscapes for different strengths of lattice potentials V_1 and V_2 are depicted in Fig. 5. Specifically, figures 5(a)–5(e) show the energy landscape as a function of the cavity field quadratures $Q = \langle \hat{Q} \rangle$ and $P = \langle \hat{P} \rangle$. It is clearly seen in Fig. 5(a) that the energy minima appears at $\langle \hat{a} \rangle = 0$ in the normal phase. Figures 5(b) and 5(e) indicate the system enters SR_1 and SR_2, respectively, and suggest that the energy minimum appears on the real axis in the SR_1 and on the imaginary axis in the SR_2. The transition between the normal phase and superradiant phase is a second-order phase transition, because there is only one energy minimum in the global plane and the transition occurs when α varies continuously across zero. Figures 5(c)–5(d) describe the case there are two differ-

ent minima located at the quadratures Q and P axes. As small changes in tuning parameters occur, the energy can eventually run from the local minima to the global minima, and the accompanying exchange of the phase of the cavity light field reveals collective excitations from one superradiant phase to another. The distributions of the energy landscapes in Figs. 5(c) and 5(d) show that there is no competition for mixed phase on gray regions in Figs. 4(d) and 4(f).

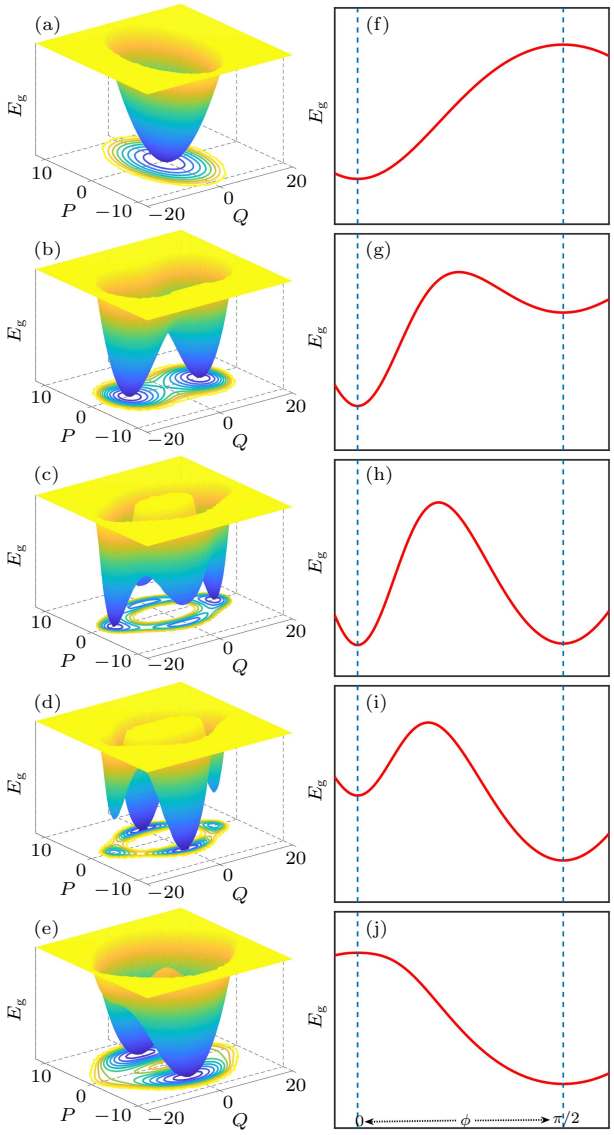


Fig. 5. (a)–(e) The ground-state energy as a function of $Q = \langle \hat{Q} \rangle$ and $P = \langle \hat{P} \rangle$ for certain V_1 and V_2. The lowest point represents a global energy minimum. (f)–(j) The energy along the circular path connecting the real and the imaginary minima, parameterized with the phase ϕ. The images are plotted at the vicinity of the critical point of transition between SR_1 and SR_2. The dark–yellow regions have larger energies as shown in panels (a)–(e), but they are not labeled with specific values.

Figures 5(f) and 5(j) show the energy of ground state on the elliptic path connecting the real and imaginary minima, parameterized with the phase ϕ. Obviously, in SR_1 region far away from the boundary of SR_1 and SR_2, there is no local minimum for the phase $\phi = \pi/2$ of the cavity photons. Slowly moving towards the critical point, a local energy minimum develops and equilibrates with that of the phase $\phi = 0$. Further increasing the pump strength, the energy swap from the local minimum to the global minimum, and eventually the local minimum for real α will vanish. Distinguishing superradiance SR_1 from SR_2 via the phase ϕ can be understood in terms of energy, the value equaling to 0 or $\pi/2$ causes the system to have a local and global minimal energies, and the first-order phase transition of the system occurs when local and global minima swap.

5. Conclusion

We have considered a system of cavity–atom hybridization irradiated by two pump fields, and have thoroughly investigated the difference between the pumps composed of pure standing waves ($\gamma = 1$) and the pumps composed of standing and running waves ($\gamma \neq 1$). By formulating and solving self-consistent mean-field equations, we obtained order parameters of the system and constructed ground-state phase diagrams spanned by the pump lattice depths V_1/E_r and V_2/E_r. Besides the normal phase, we found that the superradiant phase can be further subdivided into SR_1 with $\phi = 0$ and SR_2 with $\phi = \pi/2$. We identified that SR_1 couples to the standing wave pumps via $\sum_j \cos(\boldsymbol{k}_j \cdot \boldsymbol{r})$ and SR_2 couples to the running wave pumps via $\sum_j \sin(\boldsymbol{k}_j \cdot \boldsymbol{r})$. In addition, we calculated susceptibilities χ_1 and χ_2 to determine the tendency of the normal phase to enter into superradiance SR_1 and SR_2, respectively, and obtained the phase transition condition in terms of the cavity field quadratures acting as real and imaginary axes. We found the phase transition between the normal phase and superradiance is the second order, while the phase transition between SR_1 and SR_2 is the first order. In particular, approaching the critical point of the two superradiant phases, the ground-state energy will have a local minimum and a global minimum, and the two energy minima become equal at the critical point. When the local and global energy minima swaps, the system undergoes the first-order phase transition.

Our approach is feasible for studying the phase transition in such a cavity-BEC system, but the study of the first-order phase transition cannot be quantitatively analyzed due to the difficulty of finding suitable formulas to simulate the simultaneous occurrence of two minima on the orthogonal axes. In this study, the phase boundaries also depend on the relative spatial phase Φ between different pump and cavity fields, and here we have assumed that Φ is zero. For nonzero Φ, the new Hamiltonian now depends on it.[47,51] Of course, altering the type of particles in the cavity is also interesting for discussing many-body phases.[52–56] Encouragingly, loading ultracold quantum gases into high-finesse cavities provides a versatile platform to explore structural phase transitions between different crystal configurations, since this leads to the cavity-mediated long-range interaction between atoms and different kinds of long-range interaction support different

spatial structures in both light and atomic wave functions. We believe that our approach is favorable to the study of phase diagrams in cavity–atoms system and to the understanding of phase transitions from the energy point of view.[23]

Acknowledgements

Project supported by the National Natural Science Foundation of China (Grant Nos. 12174055 and 11674058) and the Natural Science Foundation of Fujian Province, China (Grant No. 2020J01195).

References

[1] Ritsch H, Domokos P, Brennecke F and Esslinger T 2013 *Rev. Mod. Phys.* **85** 553
[2] Vaidya V D, Guo Y, Kroeze R M, Ballantine K E, Kollár A J, Keeling J and Lev B L 2018 *Phys. Rev. X* **8** 011002
[3] Mivehvar F, Piazza F, Donner T and Ritsch H 2021 *Advances in Physics* **70** 1
[4] Zhang X, Chen Y, Wu Z, Wang J, Fan J, Deng S and Wu H 2021 *Science* **373** 1359
[5] Kongkhambut P, Skulte J, Mathey L, Cosme J G, Hemmerich A and Kebler H 2022 *Science* **377** 670
[6] Dreon D, Baumgärtner A, Li X, Hertlein S, Esslinger T and Donner T 2022 *Nature* **608** 494
[7] Helson V, Zwettler T, Mivehvar F, Colella E, Roux K, Konishi H, Ritsch H and Brantut J P 2023 *Nature* **618** 716
[8] Fraxanet J, Dauphin A, Lewenstein M, Barbiero L and González-Cuadra D 2023 *Phys. Rev. Lett.* **131** 263001
[9] Masalaeva N, Ritsch H and Mivehvar F 2023 *Phys. Rev. Lett.* **131** 173401
[10] Skulte J, Kongkhambut P, Rao S, Mathey L, Keßler H, Hemmerich A and Cosme J G 2023 *Phys. Rev. Lett.* **130** 163603
[11] Yan Z, Ho J, Lu Y H, Masson S J, Asenjo-Garcia A and Stamper-Kurn D M 2023 *Phys. Rev. Lett.* **131** 253603
[12] Young D J, Chu A, Song E Y, Barberena D, Wellnitz D, Niu Z, Schäfer V M, Lewis-Swan R J, Rey A M and Thompson J K 2024 *Nature* **625** 679
[13] Marsh B P, Kroeze R M, Ganguli S, Gopalakrishnan S, Keeling J and Lev B L 2024 *Phys. Rev. X* **14** 011026
[14] Finger F, Rosa-Medina R, Reiter N, Christodoulou P, Donner T and Esslinger T 2024 *Phys. Rev. Lett.* **132** 093402
[15] Baumann K, Guerlin C, Brennecke F and Esslinger T 2010 *Nature* **464** 1301
[16] Mottl R, Brennecke F, Baumann K, Landig R, Donner T and Esslinger T 2012 *Science* **336** 1570
[17] Norcia M A, Lewis-Swan R J, Cline J R K, Zhu B, Rey A M and Thompson J K 2018 *Science* **361** 259
[18] Mivehvar F, Ritsch H and Piazza F 2019 *Phys. Rev. Lett.* **122** 113603
[19] Defenu N, Donner T, Macrì T, Pagano G, Ruffo S and Trombettoni A 2023 *Rev. Mod. Phys.* **95** 035002
[20] Wu Z, Fan J, Zhang X, Qi J and Wu H 2023 *Phys. Rev. Lett.* **131** 243401
[21] Baumann K, Mottl R, Brennecke F and Esslinger T 2011 *Phys. Rev. Lett.* **107** 140402
[22] Klinder J, Keßler H, Bakhtiari M R, Thorwart M and Hemmerich A 2015 *Phys. Rev. Lett.* **115** 230403
[23] Li X, Dreon D, Zupancic P, Baumgärtner A, Morales A, Zheng W, Cooper N R, Donner T and Esslinger T 2021 *Phys. Rev. Res.* **3** L012024
[24] Nie X and Zheng W 2023 *Phys. Rev. A* **108** 043312
[25] Nagy D, Szirmai G and Domokos P 2008 *Eur. Phys. J. D* **48** 127
[26] Piazza F, Strack P and Zwerger W 2013 *Ann. Phys.* **339** 135
[27] Chen Y, Liu M and Chen X 2023 *Chin. Phys. B* **32** 104213
[28] Zupancic P, Dreon D, Li X, Baumgärtner A, Morales A, Zheng W, Cooper N R, Esslinger T and Donner T 2019 *Phys. Rev. Lett.* **123** 233601
[29] Tan H, Han J, Zheng W, Yuan J and Li Y 2022 *Phys. Rev. A* **106** 023315
[30] Bhaseen M J, Mayoh J, Simons B D and Keeling J 2012 *Phys. Rev. A* **85** 013817
[31] Piazza F and Ritsch H 2015 *Phys. Rev. Lett.* **115** 163601
[32] Léonard J, Morales A, Zupancic P, Donner T and Esslinger T 2017 *Science* **358** 1415
[33] Léonard J, Morales A, Zupancic P, Esslinger T and Donner T 2017 *Nature* **543** 87
[34] Mivehvar F, Ostermann S, Piazza F and Ritsch H 2018 *Phys. Rev. Lett.* **120** 123601
[35] Morales A, Zupancic P, Léonard J, Esslinger T and Donner T 2018 *Nat. Mater.* **17** 686
[36] Qin W, Zheng D C, Wu Z D, Chen Y H and Liao R 2024 *Phys. Rev. A* **109** 013310
[37] Wu B H, Yang X X, Chen Y and Zhang W 2024 *Chin. Phys. Lett.* **41** 064201
[38] Klinder J, Kebler H, Wolke M, Mathey L and Hemmerich A 2015 *PNAS* **112** 3290
[39] Landini M, Dogra N, Kroeger K, Hruby L, Donner T and Esslinger T 2018 *Phys. Rev. Lett.* **120** 223602
[40] Morales A, Dreon D, Li X, Baumgärtner A, Zupancic P, Donner T and Esslinger T 2019 *Phys. Rev. A* **100** 013816
[41] Zhai H 2021 *A Single Atom* (Cambridge University Press) pp. 3–30
[42] Piazza F and Ritsch H 2015 *Phys. Rev. Lett.* **115** 163601
[43] Ali A, Saif F and Saito H 2022 *Phys. Rev. A* **105** 063318
[44] Gao P, Zhou Z W, Guo G C and Luo X W 2023 *Phys. Rev. A* **107** 023311
[45] Sachdev S 2011 *Quantum Phase Transitions*, 2nd edn. (Cambridge University Press)
[46] Lifshitz E and Pitaevskii L 2013 *Statistical Physics: Theory of the Condensed State* (Course of Theoretical Physics Vol. 9 Book 2) (Butterworth-Heinemann)
[47] Press W H, Teukolsky S A, Vetterling W T and Flannery B P 2007 *Numerical Recipes with Source Code CD-ROM* 3*rd Edition: The Art of Scientific Computing* (USA: Cambridge University Press) ISBN 0521884071
[48] Ali A, Saif F and Saito H 2022 *Phys. Rev. A* **105** 063318
[49] Gao P, Zhou Z W, Guo G C and Luo X W 2023 *Phys. Rev. A* **107** 023311
[50] Tan H, Cao R and Li Y Q 2023 *Acta Phys. Sin* **72** 183701 (in Chinese)
[51] Fan J, Chen G and Jia S 2020 *Phys. Rev. A* **101** 063627
[52] Keeling J, Bhaseen M J and Simons B D 2014 *Phys. Rev. Lett.* **112** 143002
[53] Chen Y, Yu Z and Zhai H 2014 *Phys. Rev. Lett.* **112** 143004
[54] Piazza F and Strack P 2014 *Phys. Rev. Lett.* **112** 143003
[55] Chen Y, Zhai H and Yu Z 2015 *Phys. Rev. A* **91** 021602
[56] Kollath C, Sheikhan A, Wolff S and Brennecke F 2016 *Phys. Rev. Lett.* **116** 060401